arXiv:1701.04542v2 [cond-mat.str-el] 21 Jan 2017

Chiral Phase Transitions in a Metallic Frustrated Magnet

Munir Shahzad and Pinaki Sengupta
School of Physical and Mathematical Sciences, Nanyang Technological University, 21 Nanyang Link, Singapore 637371
(Dated: January 24, 2017)

We explore the magnetic phases in a Kondo lattice model on the geometrically frustrated Shastry-Sutherland lattice at metallic electron densities, searching for topologically non-trivial chiral spin textures. Motivated by experimental observations in many rare earth based frustrated metallic magnets, we treat the local moments as classical spins and set the coupling between the itinerant electrons and local moments as the largest energy scale in the problem. Our results show that a canted flux state with non-zero static chirality is stabilized over an extended range of Hamiltonian parameters. The chiral spin state can be quenched efficiently by external fields like temperature and magnetic field as well as by varying the degree of frustration in the electronic itinerancy. Interestingly, unlike insulating electron densities, a Dzyaloshinskii-Moriya interaction between the local moments is not essential for the emergence of their non-coplanar ordering.

I. INTRODUCTION

The interplay between charge and spin degrees of freedom results in various novel and exotic phases in strongly correlated electron systems. A paradigmatic model to describe this interplay is the Kondo lattice model (KLM) or double exchange model (DEM) in which localized moments are coupled to itinerant electrons[1–5]. The mobile electrons in these systems act as mediators to establish the effective correlation between localized spins giving rise to magnetic behavior. On the other hand the scattering of these electrons from localized moments may affect the electronic and transport properties of these systems. The study becomes more fascinating when we have geometrical frustration as an extra degree of freedom like the hybrid systems in which localized spins are arranged on geometrically frustrated lattices. These charge-spin coupled systems on frustrated lattices exhibit chiral spin textures that drive novel and exotic topological properties[6–10]. For these non-coplanar spin configurations the scalar spin chirality defined on a triangle $\chi_{\triangle} = \mathbf{S}_i \cdot \mathbf{S}_j \times \mathbf{S}_k$ is non-zero. The non-zero value of chirality breaks both time-reversal ($\mathbf{T}$) and parity ($\mathbf{P}$) symmetries and drives some peculiar transport phenomena such as geometrical or Topological Hall effect (THE)[11–16]. These chiral spin configurations act as a source of fictitious magnetic field–when an itinerant electron moves over them in a closed path it picks up an extra Berry phase which results in THE[17–20]. THE has been studied for Ferromagnetic Kondo lattice model on geometrically frustrated lattices such as triangular[21–24], kagome[20,25,26], checkerboard[27], pyrochlore[28,29] and face-centered cubic lattice[30]. Chiral spin textures are essential in realizing this novel transport phenomena.

The topological nature of chiral spin textures emerging dynamically from the interplay between competing microscopic interactions can be controlled with the help of external magnetic field, temperature and pressure which make them a potential candidate for application in spintronics. So it is very desirable to study the topological nature of these magnetic ordered states and associated phase transitions in order to stimulate experimental work. In this work, we investigate the SS-KLM for the stabilization of topologically non-trivial ground states at one-quarter and three-quarter filling of itinerant electrons, for which the ground state is metallic. Our results reveal that non-coplanar ground states are stabilized for a wide range of parameters involved in the Hamiltonian. We discuss in detail the nature of topological phase transition as a function of thermal fluctuations, frustration and external magnetic field for both number densities of electrons.

II. MODEL

We consider the SS-KLM in the presence of a longitudinal magnetic field. The geometry of SSL along with the first Brillouin Zone (BZ) is depicted in Fig. 1. The Hamiltonian describing the system under investigation is,

$$\hat{\mathcal{H}} = \underbrace{-\sum_{\langle i,j\rangle,\sigma} t_{ij}(c^{\dagger}_{i\sigma}c_{j\sigma} + h.c.) - J_K \sum_i \mathbf{S}_i \cdot \mathbf{s}_i}_{\hat{\mathcal{H}}_e} + \underbrace{\sum_{\langle i,j\rangle} J_{ij}\mathbf{S}_i \cdot \mathbf{S}_j - h^z \sum_i S^z_i}_{\hat{\mathcal{H}}_c} \quad (1)$$

The first two terms make up the electronic part of the Hamiltonian $\hat{\mathcal{H}}_e$ where we have a tight binding term for itinerant electron and a Kondo-like interaction between these electrons and localized spins. $\langle i,j\rangle$ denotes the bonds on the SSL, where nearest neighbors (NN) are axial bonds and next nearest neighbors (NNN) are diagonal bonds on the alternate plaquette and t_{ij} describes the hopping matrix of itinerant electrons on these SSL bonds. We treat the localized spins $\mathbf{S}_i$ as classical vectors of unit length so the sign of J_K becomes irrelevant in the current model. The third term in Eq. (1) represents anti-ferromagnetic Heisenberg interaction between the localized spins. The last term in the Hamiltonian (1)

is the Zeeman term for the localized spins due to an external (longitudinal) magnetic field. We consider the strong J_K coupling limit, in that case, the spin direction of itinerant electron is completely determined by the localized moment. So we just consider the effect of an external magnetic field on the localized moments only. From here onwards, we represent the interactions on the axial bonds as unprimed parameters while primed for diagonals bonds. We choose $t = 1$ as the energy unit. In an accompanying work[31], we have investigated the role of Dzyaloshinskii-Moriya (DM) interactions on stabilizing chiral spin textures at half-filling, where there exists a finite gap in the electronic spectrum. We found that for the insulating state, DM interactions are essential in establishing non-coplanar ordering of the local moments. In this work, we focus on electronic filling factors $n_e = \frac{1}{4}$ and $\frac{3}{4}$ – where $n_e = \frac{1}{2N}\sum_i c_i^\dagger c_i$ and N is the number of lattice sites – for which the electronic spectrum is gapless, i.e., the ground state is metallic. We demonstrate that at these parameter regimes, topologically non-trivial chiral spin textures emerge even in the absence of DM interactions. Here we report the results of our study on the effects of temperature, frustration and magnetic field on the emergent chiral spin orderings.

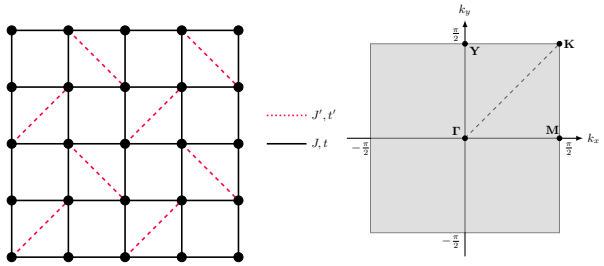

(a) (b)

FIG. 1. (Color online) (a) The Geometry of SSL, where there are diagonal bonds on alternate plaquette in addition to axial bonds along x and y-axis. (b) 1st BZ of SSL lattice with high symmetric points mentioned.

III. METHOD AND OBSERVABLES

The above model can be explored for thermodynamic properties by using an unbiased Monte Carlo (MC) method. This approach has already been used in similar type of studies[21,32–35]. We will present a brief introduction of this method in accordance with the main references[36,37]. We can separate and hence decouple the slow dynamics of the localized spins of rare earth ions from the fast dynamics of the itinerant electrons. In this case, the local moments at each site can be treated as classical static adiabatical fields. By replacing the itinerant electron spin as $\mathbf{s}_i = c^\dagger_{i,\alpha}\boldsymbol{\sigma}_{\alpha\beta}c_{i,\beta}$, the electronic part of the Hamiltonian $\hat{\mathcal{H}}_e$ becomes quadratic in fermionic operators where $\boldsymbol{\sigma}_{\alpha\beta}$ are the vector elements of usual Pauli matrices. The localized spin are defined as $\mathbf{S}_i = (\sin\theta_i\cos\phi_i, \sin\theta_i\sin\phi_i, \cos\theta_i)$ with $|\mathbf{S}_i| = 1$. The one-electron basis can be used to express $\hat{\mathcal{H}}_e$ as $2N \times 2N$ matrix for a particular arrangement of classical localized spins.

To study the thermodynamic properties the full partition function in the grand canonical ensemble is represented in terms of two traces,

$$Z = \mathrm{Tr}_c\mathrm{Tr}_f \exp[-\beta(\hat{\mathcal{H}}_e(\{x_r\}) - \mu n_e)]\cdot \exp[-\beta(\hat{\mathcal{H}}_c)]. \quad (2)$$

In above equation, Tr_c and Tr_f are traces over the classical localized moments, $\{x_r\}$, and fermionic degrees of freedom respectively. The eigenvalues of the Hamiltonian matrix $\hat{\mathcal{H}}_e$ for a fixed configuration of the localized spins are used to calculate the trace Tr_f,

$$\mathrm{Tr}_f \exp[-\beta(\hat{\mathcal{H}}_e(\{x_r\}) - \mu n_e)] = \prod_\nu (1 + \exp[-\beta(\varepsilon_\nu(\{x_r\}) - \mu)]) \quad (3)$$

where $\beta = 1/k_BT$ is the inverse temperature and μ is the chemical potential. Using Eq. (3) the full partition function can be written as,

$$Z = \mathrm{Tr}_c \exp[-S_{\mathit{eff}}(\{x_r\}) - \beta(\hat{\mathcal{H}}_c)] \quad (4)$$

where $S_{\mathit{eff}}(\{x_r\}) = \sum_\nu F(y)$ is the effective action and $F(y) = -\log[1 + \exp\{-\beta(y-\mu)\}]$. To calculate Tr_c a classical MC method is used to sample the spin configuration space. We can write the probability distribution for a fixed configuration of localized moments $\{x_r\}$ as,

$$P(\{x_r\}) \propto \exp[-S_{\mathit{eff}}(\{x_r\}) - \beta(\hat{\mathcal{H}}_c)] \quad (5)$$

The eigenvalues and eigenfunctions of $\hat{\mathcal{H}}_e(\{x_r\})$ are used to calculate the thermodynamic quantities related to itinerant electrons while the quantities associated with the localized spins are calculated by the thermal averages of spin configurations. We select a random configuration of localized spin $\{x_r\}$ and calculate the Boltzmann action $S_{\mathit{eff}}(\{x_r\})$ for this configuration. Next, the random updates performed to this spin configuration are accepted or rejected based on Metropolis algorithm. We use the magnetization per unit site and static spin structure factor to distinguish between different magnetic orders of the localized spins,

$$S(\mathbf{q}) = \frac{1}{N}\sum_{i,j}\langle \mathbf{S}_i \cdot \mathbf{S}_j\rangle \exp[i\mathbf{q}\cdot\mathbf{r}_{ij}] \quad (6)$$

where $\langle\rangle$ represent the thermal averages over the grand canonical ensemble and $\mathbf{r}_{ij}$ is the position vector from

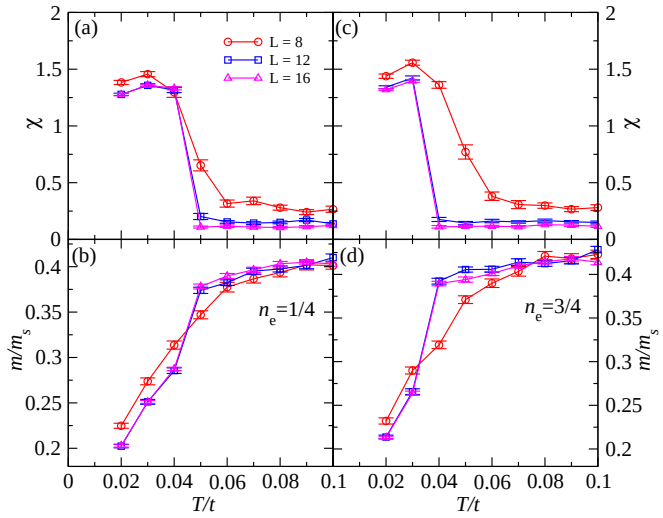

FIG. 2. (Color online) Plots of magnetization per unit site (upper panels) and chirality (lower panels) as a function of temperature T at $n_e \simeq 1/4$ (left) and 3/4 (right). The parameters used are $t' = 0.25$, $J = 0.1$, $J' = 0.025$, $h^z = 0$ and $J_K = 8.0$.

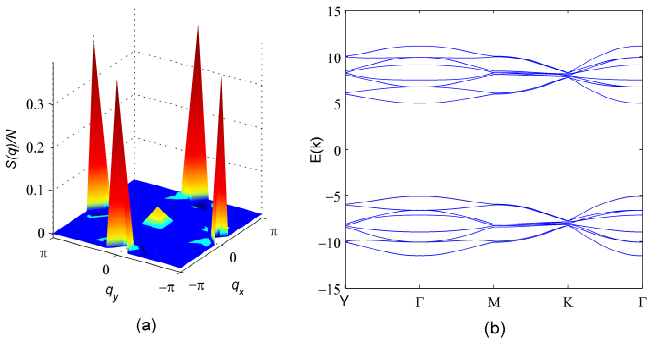

FIG. 3. (Color online) (a) The momentum dependence of static spin structure factor exhibiting sharp peaks at $\mathbf{q} = (0, \pi)$, $(\pi, 0)$ and a small peak at $(0, 0)$. The results are obtained using parameters $t' = 0.25$, $J = 0.1$, $J' = 0.025$, $h^z = 0$, $J_K = 8.0$ and $T = 0.02$ for 12×12 lattice at $n_e \simeq 1/4$. (b) Electronic energy bands for a tight binding model including double exchange interaction with triple-$\mathbf{q}$ order stabilized at $\mathbf{q} = (\pi, 0)$, $(0, \pi)$ and $(0, 0)$. The values of interaction parameters used are $t = 1.0$, $t' = 0.25$ and $J_K = 8.0$

site i to j. We use the total chirality $\chi = \frac{1}{N_u} \sum_{\triangle} \chi_{\triangle}$ to differentiate between topological trivial and non-trivial magnetic states, where the sum is taken over all the triangles made on the alternate plaquettes with diagonal bonds and N_u is the number of unit cells of SSL. The value of the chiral order parameter is non-zero for *non-coplanar* configurations such as all-out, 2-in 2-out and 3-in 1-out while it is zero for coplanar magnetic states such as anti-ferromagnetic (AFM), ferromagnetic (FM), stripe and pure flux states.

IV. RESULTS AND DISCUSSIONS

We have done calculations for lattice size $L = 8 - 16$, where L is the length of the lattice along one axis. The results for $L = 8$ are obtained by diagonalizing the full Hamiltonian to calculate the Boltzmann factor as it is faster for small lattice sizes. But for lattice size $L > 8$, we used the travelling cluster approximation (TCA)[38–41], in this method, a cluster of 6×6 sites is moved sequentially over the whole lattice and Boltzmann factor was calculated by just diagonalizing this cluster Hamiltonian. Once the system is equilibrated then physical observables are calculated by diagonalizing the full Hamiltonian. To approach equilibration efficiently and avoid getting stuck at any local minimum, we have used a simulated annealing method. At the beginning, we select a random configuration of the localized spins at a relatively high temperature $T = 0.1$ and equilibrate the system. Next, we use the final configuration of this temperature to do the equilibration at $T = 0.08$. This process is repeated with a temperature step, $\Delta T = 0.02$, finally measuring the thermal averages of the physical observables at $T = 0.02$. Measurements are made after every $1,000$ steps of an MC run of $40,000$ steps in total after discarding $2000 - 60,000$ MC steps for thermalization. We have divided the data into 40 different bins to calculate the average value and error from the standard deviation.

A. Role of Temperature

Throughout this work we choose the limit of strong Kondo coupling between itinerant electrons and localized spins ($J_K = 8.0$) following the experimental observations in relevant metallic magnets. We start our discussion by considering the thermal transition of the magnetic ground state. Fig. 2 (a) and (b) show the temperature dependence of magnetization and scalar spin chirality as a function of temperature at $n_e \simeq 1/4$ (here we have introduced $\simeq$ sign because we are working in grand canonical ensemble and electron densities are controlled by the values of μ give number densities fluctuating within the error bars close to the required density). Initially, the magnetization decreases very slowly with decreasing temperature but around $T \simeq 0.05$ there is a discontinuous drop in magnetization indicating a first order magnetic phase transition. The nature of this transition becomes much clearer if we look at Fig. 2 (b) where we have shown the behavior of chirality while varying T for $n_e \simeq 1/4$. The value of chirality is very small and it remains almost flat at higher values of temperature indicating an absence of non-coplanar ordering. The non-zero value of chirality in this limit can be attributed to thermal fluctuations which are dominant at higher temperatures. But as we approach $T \simeq 0.05$ a transition to a non-coplanar spin ordering is indicated by a discontinuous increase in the value of χ as seen in Fig. 2 (b). At lower temperatures, χ approaches a finite value – signalling a chiral

phase. These results clearly demonstrate the chiral symmetry breaking character of the transition. Quenching the thermal fluctuations drives the system from a topologically trivial paramagnet to a topologically non-trivial state marked by finite chirality at low temperature.

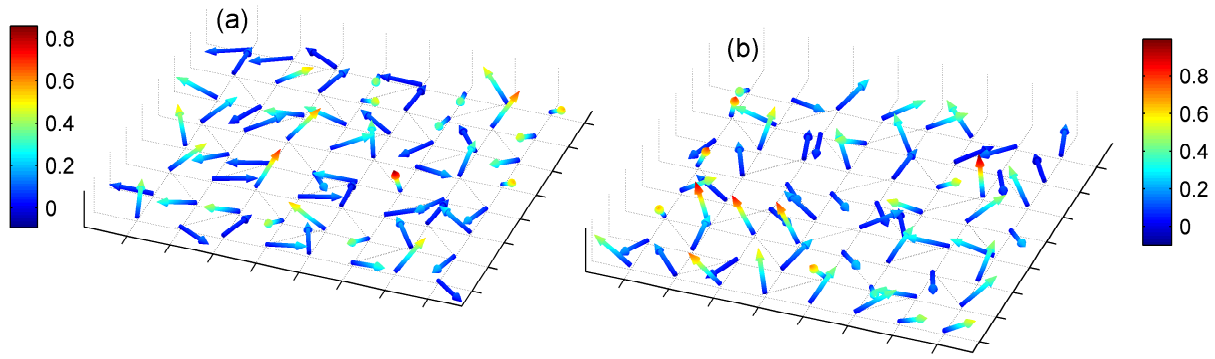

FIG. 4. (Color online) Real space configurations of localized spins obtained from MC calculations on 8×8 lattice (a) when $T = 0.03$, after the phase transition and (b) when $T = 0.06$, prior to phase transition. The data is obtained for $n_e \simeq 1/4$ when $t' = 0.25$, $J = 0.1$, $J' = 0.025$, $h^z = 0$ and $J_K = 8.0$.

What is the nature of the ordered state? Insight into the nature of the magnetic ordering can be gained from a plot of the static spin structure factor, $S(\mathbf{q})$ as a function of the momentum [see Fig. 3(a)]. It consists of sharp peaks at $\mathbf{q} = (\pi, 0)$ and $(0, \pi)$ and a sub-dominant peak at $\mathbf{q} = (0, 0)$. The dual peaks at $(\pi, 0)$ and $(0, \pi)$ is a signature of flux state in similar models. The in-plane components of the local moments are arranged in a flux pattern. The central peak indicates a canting of the moments out of the plane. In other words, the magnetic ground state is a canted flux state. This is confirmed by snapshots of the local spin configurations above and below the transition temperature [Fig. 4]. At higher temperatures, the local moments are in a paramagnetic state. In the ordered state, the local moments are oriented with their transverse components forming a flux pattern around the squares with no diagonal - with alternate clockwise and counter-clockwise circulation around neighboring plaquettes. There is a net longitudinal component as the double exchange interaction favors ferromagnetic ordering at this filling. The real space configurations of localized spins also established the fact that the magnetic ground state is a canted flux phase. This canted flux state is stabilized due the competition between AFM super-exchange interaction and the double exchange interaction (that favors the FM ordering at this filling factor) in the presence of geometrical frustration.

Next we move to $n_e \simeq 3/4$ case, we have illustrated the results obtained from MC calculations for magnetization per site and chirality while varying T in Fig. 2 (c) and (d) respectively. A chiral phase transition similar to the case for $n_e \simeq 1/4$ is also observed here. However, finite size effects are much more pronounced for $n_e \simeq 3/4$ as seen in Fig. 2 (c) and (d). The approach to thermodynamic limit occurs much more slowly with system size. The ground state at the lower temperature is canted flux state similar to the previous case. This similarity between the results for both cases can be ascribed to the symmetry of band structure at one-quarter and three-quarter filling of itinerant electrons. In Fig. 3 (b) the electronic energy bands along symmetric points in BZ are shown for

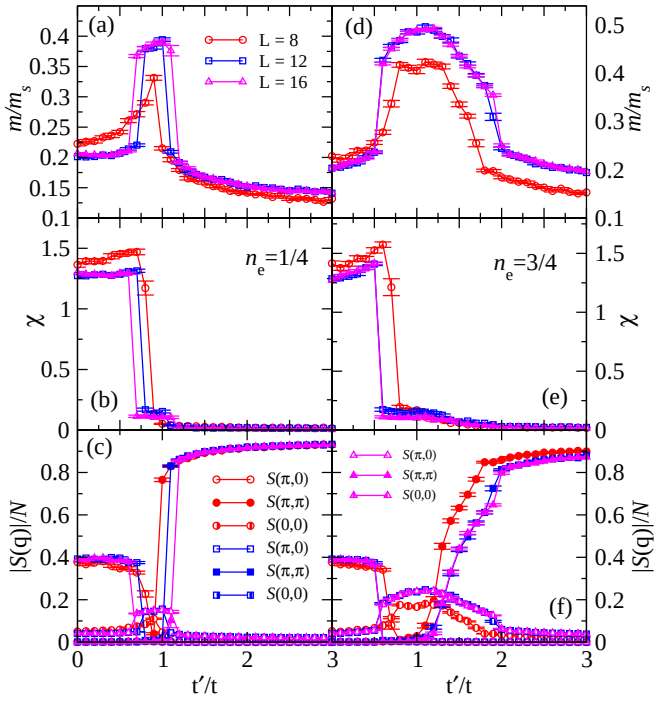

FIG. 5. (Color online) Frustration dependence of magnetization per site, chirality and static structure factor at $\mathbf{q} = (0, 0), (\pi, 0)$ and (π, π) at $n_e \simeq 1/4$ and $3/4$. The calculations are done keeping the values of parameters $J = 0.1$, $J' = 0.025$, $h^z = 0$, $J_K = 8.0$ and $T = 0.02$.

a tight-binding model with a double exchange term and a triple-Q ordering of the local moments. The three values of $\mathbf{q}$ used are that of canted flux state – $(0,\pi)$, $(\pi,0)$ and $(0,0)$. It is clear that the bands are symmetric for one-quarter and three-quarter filling of electron density.

B. Role of Frustration

Now we explore the role of frustration on the magnetic properties of the current model. Since t' and J' are determined by the overlap of different orbitals across the diagonal bonds, their ratio can, in principle, be different for different materials. In this study, we choose to vary t', keeping J' constant. Both t' and J' induce frustration – the former in electron hopping and the latter in exchange interactions between local moments. With varying t', the nature of electron hopping changes from being unfrustrated at $t'=0$ to highly frustrated at $t' \gtrsim t$, whereas the degree of frustration in the direct exchange between the local moments remain unaltered. We start with $n_e \simeq 1/4$ – Fig. 5 (a) and (b) show the results of MC calculations for magnetization and chirality while varying the hopping integral on the diagonal bonds t'. At $t'/t = 0.0$ the ground state has a non-zero magnetization and finite chirality. The static spin structure factor for this state exhibits a small peak at $\mathbf{q} = (0,0)$ in addition to two sharp and equal in magnitude peaks at $(0,\pi)$ and $(\pi,0)$. Actually this is the same canted flux state that we encountered earlier. The in-plane components of the local moments are arranged in a pattern similar to a coplanar Flux state. Furthermore, the moments are tilted slightly out-of-plane due to geometrical frustration (in Heisenberg interaction) and competition between FM double exchange interaction and AF Heisenberg interaction.

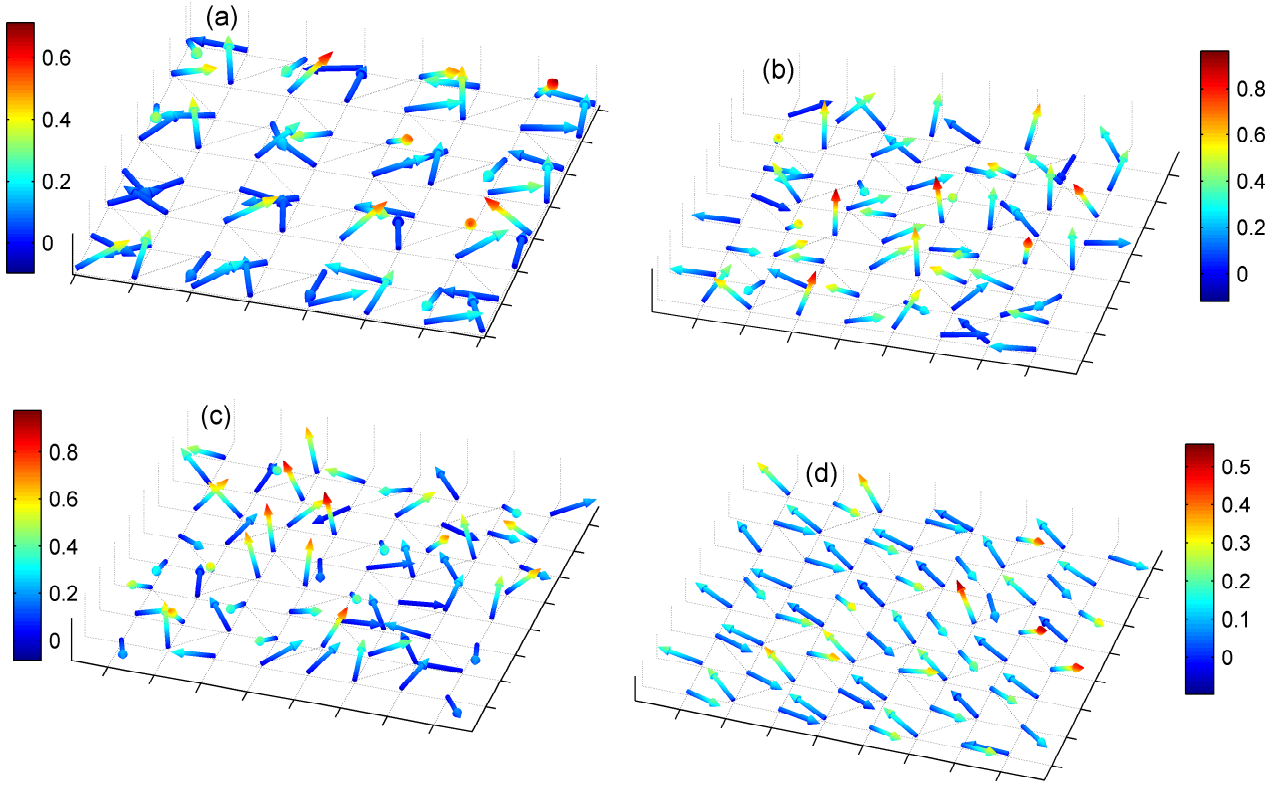

FIG. 6. (Color online) The equilibrium real space spin configurations obtained from MC calculations on 8×8 lattice (a) when $t'/t = 0.2$, before the 1st phase transition and (b) when $t'/t = 0.8$, after 1st phase transition (c) when $t'/t = 1.0$, just before 2nd phase transition and (d) when $t'/t = 2.2$, after the 2nd phase transition. The data is obtained for $n_e \simeq 3/4$ case when $J = 0.1$, $J' = 0.025$, $h^z = 0.0$ and $J_K = 8.0$ at $T = 0.02$. See text for more details about these two phase transitions.

The flux pattern consists of columnar AFM arrangements of the in-plane components with simultaneous $(\pi,0)$ and $(0,\pi)$ ordering. With increasing t'/t, the magnetization remains constant at a value consistent with a canted flux state up to $t'/t \approx 0.75$, where there is a discontinuous transition to a state with partial polarization of the spins. m/m_s jumps to ≈ 0.4 and remains constant for $0.75 \lesssim t'/t \gtrsim 1.0$. In this intermediate range of t'/t, the flux ordering is broken and the transverse components of the local moments are fully disordered. The strength of the static structure factor $S(\mathbf{q})$ is vanishingly small for the AFM ordering wave vectors $(\pi,0)$,

$(0,\pi)$ and (π,π) indicating the complete suppression of AFM ordering. This breaking of in-plane flux ordering results in an increase in the partial ordering of the longitudinal component, reflected in the increased magnetization. The chirality drops discontinuously to a very small value as a result of the breaking of the flux pattern. Upon further increasing t'/t there is a second discontinuous spin-flop transition to a canted AFM state with small magnetization. The in-plane components of the local moments are arranged in a staggered (π,π) order with a small out-of-plane component resulting from the strong double-exchange interaction. The chirality is suppressed completely indicating a pure AFM character of the ground state spin configuration. The nature of the magnetic ground states in the different regimes is, once again, confirmed by the snapshots of instantaneous spin configurations shown in Fig. 6 [shown here for $n_e = 3/4$ case]. The in-plane components are seen to evolve from a flux pattern at small t'/t to completely disordered in the intermediate regime to staggered AFM order at large values of t'/t.

The evolution of the magnetic ground state with changing t'/t is qualitatively the same for $n_e = 3/4$, as seen in Fig. 5 (d) and (e). The range of the intermediate state is much larger. We plan to investigate the nature of this intriguing state further in future studies.

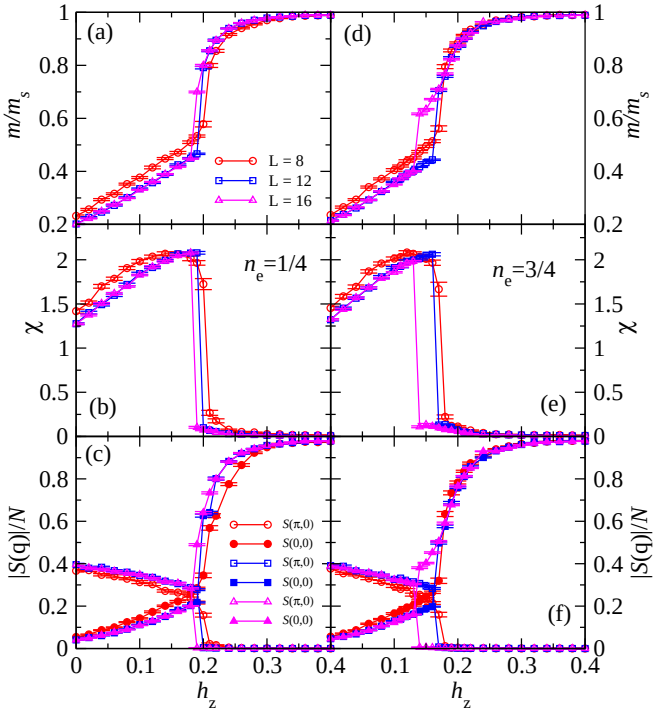

FIG. 7. (Color online) The magnetic field dependence of magnetization per site, chirality and static structure factor at $\mathbf{q} = (0,0), (\pi,0)$ and (π,π) at $n_e \simeq 1/4$ and $3/4$. The calculations are done keeping the values of parameters $t' = 0.25$, $J = 0.1$, $J' = 0.025$, $J_K = 8.0$ and $T = 0.02$.

C. Role of Magnetic Field

Finally, we investigate the role of external magnetic field in the current model both at one-quarter and three-quarter fillings of electrons. Applying an external field is the simplest and most direct way of controlling the magnetic character of a system. Our goal is to explore the tunability of the chiral spin states by applying a static, uniform, longitudinal external field. For $n_e \simeq 1/4$ the magnetic field dependence of magnetization and chirality is shown in Fig. 7 (a) and (b) respectively. At $h^z = 0.0$ the magnetic ground state is canted flux state which we have already discussed in detail. The uniform magnetization is non-zero at zero field even though the direct exchange between the local moments are AFM in nature. This is due to the strong coupling between the local moments and the itinerant electrons. The magnetization m/m_s increases monotonically up to $h_z = 0.2$ when there is an abrupt jump in its value from ≈ 0.45 to ≈ 0.8, marking a field driven discontinuous transition. The chirality, which is finite in the canted flux state ($h_z < 0.2$), is broken at the transition, establishing the chiral nature of the field induced transition. Indeed the transition marks the breaking of the flux pattern of the in-plane components of the local moments. This is confirmed by the behavior of the static structure factor at $(0,0)$ and $(\pi,0)$. At the transition, the peak at $(\pi,0)$ is completely suppressed, whereas the $(0,0)$ peak (proportional to the square of the uniform magnetization) exhibits a discontinuous increase in its value. With further increase in magnetic field, the system approaches full polarization asymptotically. Once again the field dependence of the magnetic ground state is qualitatively similar for $n_e = 3/4$, confirming the particle-hole symmetry of the system.

V. SUMMARY

To summarize we have studied in detail the magnetic properties of the SS-KLM at filling factors of itinerant electrons $n_e = 1/4$ and $3/4$ at which the ground state is metallic. We find that a chiral canted flux state is stabilised over a large range of parameters at both densities. Interestingly, in contrast to insulating ground states, a Dzyaloshinskii-Moriya interaction is not essential for stabilizing non-coplanar spin texture. The chiral magnetic ground state can be suppressed via a discontinuous chiral phase transition by external fields such as temperature, by a static, uniform longitudinal magnetic field, as well as by increasing the magnitude of frustration in electronic component of the Hamiltonian. In fact, tuning the strength of diagonal hopping (which is responsible for frustration) drives the magnetic ground state from a canted flux phase at small frustration to a partially polarized intermediate state at moderate frustration to a canted AFM state at large frustration. Interestingly, while both the canted flux and AFM states have AFM ordering in the transverse plane, the intermediate state

is characterized by a completely random distribution of the in-plane components. We plan to investigate this intriguing state in the near future.

ACKNOWLEDGMENTS

The work was partially supported by Grant No. MOE2014-T2-2-112 from the Ministry of Education, Singapore. We also acknowledge the use of HPC cluster at NSSC, Singapore.

[1] C. Zener, Phys. Rev. **82**, 403 (1951).
[2] P. W. Anderson and H. Hasegawa, Phys. Rev. **100**, 675 (1955).
[3] N. Furukawa, Journal of the Physical Society of Japan **64**, 2734 (1995).
[4] S. Yunoki, J. Hu, A. L. Malvezzi, A. Moreo, N. Furukawa, and E. Dagotto, Phys. Rev. Lett. **80**, 845 (1998).
[5] K. Kubo and N. Ohata, J. Phys. Soc. Jpn. **33**, 21 (1972).
[6] D. Grohol, K. Matan, J.-H. Cho, S.-H. Lee, J. W. Lynn, D. G. Nocera, and Y. S. Lee, Nat Mater **4**, 323 (2005).
[7] L. Balicas, S. Nakatsuji, Y. Machida, and S. Onoda, Phys. Rev. Lett. **106**, 217204 (2011).
[8] X. G. Wen, F. Wilczek, and A. Zee, Phys. Rev. B **39**, 11413 (1989).
[9] X. G. Wen, Phys. Rev. B **43**, 11025 (1991).
[10] R. B. Laughlin and Z. Zou, Phys. Rev. B **41**, 664 (1990).
[11] M. Udagawa and R. Moessner, Phys. Rev. Lett. **111**, 036602 (2013).
[12] D. Boldrin and A. Wills, Adv. in Cond. Matt. Phys. **2012** (2012), 10.1155/2012/615295.
[13] Y. Taguchi, Y. Oohara, H. Yoshizawa, N. Nagaosa, and Y. Tokura, Science **291**, 2573 (2001).
[14] N. Nagaosa, Mat. Sci. and Engi.: B **84**, 58 (2001).
[15] Y. Machida, S. Nakatsuji, S. Onoda, T. Tayama, and T. Sakakibara, Nature **463**, 210 (2010).
[16] Y. Machida, S. Nakatsuji, Y. Maeno, T. Tayama, T. Sakakibara, and S. Onoda, Phys. Rev. Lett. **98**, 057203 (2007).
[17] J. Ye, Y. B. Kim, A. J. Millis, B. I. Shraiman, P. Majumdar, and Z. Tešanović, Phys. Rev. Lett. **83**, 3737 (1999).
[18] M. V. Berry, in *Proceedings of the Royal Society of London A: Mathematical, Physical and Engineering Sciences*, Vol. 392 (The Royal Society, 1984) pp. 45–57.
[19] D. Loss and P. M. Goldbart, Phys. Rev. B **45**, 13544 (1992).
[20] K. Ohgushi, S. Murakami, and N. Nagaosa, Phys. Rev. B **62**, R6065 (2000).
[21] Y. Kato, I. Martin, and C. D. Batista, Phys. Rev. Lett. **105**, 266405 (2010).
[22] K. Barros and Y. Kato, Phys. Rev. B **88**, 235101 (2013).
[23] A. Rahmani, R. A. Muniz, and I. Martin, Phys. Rev. X **3**, 031008 (2013).
[24] H. Takatsu, S. Yonezawa, S. Fujimoto, and Y. Maeno, Phys. Rev. Lett. **105**, 137201 (2010).
[25] K. Barros, J. W. F. Venderbos, G.-W. Chern, and C. D. Batista, Phys. Rev. B **90**, 245119 (2014).
[26] G.-W. Chern, A. Rahmani, I. Martin, and C. D. Batista, Phys. Rev. B **90**, 241102 (2014).
[27] J. W. F. Venderbos, M. Daghofer, J. van den Brink, and S. Kumar, Phys. Rev. Lett. **109**, 166405 (2012).
[28] G.-W. Chern, Phys. Rev. Lett. **105**, 226403 (2010).
[29] S. Nakatsuji, Y. Machida, Y. Maeno, T. Tayama, T. Sakakibara, J. v. Duijn, L. Balicas, J. N. Millican, R. T. Macaluso, and J. Y. Chan, Phys. Rev. Lett. **96**, 087204 (2006).
[30] R. Shindou and N. Nagaosa, Phys. Rev. Lett. **87**, 116801 (2001).
[31] M. Shahzad and P. Sengupta, arxiv preprint 1701.04297 (2017).
[32] H. Ishizuka and Y. Motome, Phys. Rev. Lett. **108**, 257205 (2012).
[33] C. Şen, G. Alvarez, Y. Motome, N. Furukawa, I. A. Sergienko, T. C. Schulthess, A. Moreo, and E. Dagotto, Phys. Rev. B **73**, 224430 (2006).
[34] H. Ishizuka and Y. Motome, Phys. Rev. B **88**, 081105 (2013).
[35] H. Ishizuka and Y. Motome, Phys. Rev. B **91**, 085110 (2015).
[36] Y. Motome and N. Furukawa, J. Phys. Soc. Jpn. **68**, 3853 (1999).
[37] N. Furukawa and Y. Motome, J. Phys. Soc. Jpn. **73**, 1482 (2004).
[38] Kumar, S. and Majumdar, P., Eur. Phys. J. B **50**, 571 (2006).
[39] A. Mukherjee, N. D. Patel, C. Bishop, and E. Dagotto, Phys. Rev. E **91**, 063303 (2015).
[40] S. Kumar and P. Majumdar, Phys. Rev. Lett. **96**, 016602 (2006).
[41] S. Kumar and P. Majumdar, Phys. Rev. Lett. **94**, 136601 (2005).